

# Natural frequencies analysis of functionally graded circular cylindrical shells

N. Alshabat<sup>a,\*</sup>, M. Zannon<sup>b</sup>

<sup>a</sup>Mechanical Engineering Department, Tafila Technical University Tafila 66110, Jordan

<sup>b</sup>Applied Mathematics Department, Tafila Technical University Tafila 66110, Jordan

Received 11 November 2020; accepted 28 June 2021

---

## Abstract

In the present work, a study on natural frequencies of functionally graded materials (FGM) circular cylindrical shells is presented. The FGM is considered to be a mixture of two materials. The volumetric fractions are considered to vary in the radial direction (i.e., through the thickness) in compliance with a conventional power-law distribution. The equivalent material properties are estimated based on the Voigt model. The analysis of the FGM cylindrical shells is performed using the third-order shear deformation shell theory and the principle of virtual displacements. Moreover, the third-order shear deformation shell theory coupled with Carrera's unified formulation is applied for the derivation of the governing equations associated with the free vibration of circular cylindrical shells. The accuracy of this method is examined by comparing the obtained numerical results with other previously published results. Additionally, parametric studies are performed for FGM cylindrical shells with several boundary conditions in order to show the effect of several design variables on the natural frequencies such as the power-law exponent, the circumferential wave number, the length to radius ratio and the thickness to radius ratio.

© 2021 University of West Bohemia.

*Keywords:* FGM circular cylindrical shell, natural frequencies, third-order shear deformation shell theory, Carrera's unified formulation

---

## 1. Introduction

Functionally graded materials (FGMs) are composite materials made of a mixture of at least two base materials with a continuous variation of their volumetric fraction in accordance with a prescribed function. Therefore, the material properties of the FGM, such as the Young's modulus and density, continuously and smoothly vary by means of the volume. The smooth variation of the material properties overcomes the delamination problem, which is common in conventional laminated composites. The first FGM was introduced in Japan in 1984 for designing a thermal barrier to endure high-temperature gradient conditions [32]. Since then FGMs have attracted much interest in other fields such as the biomedical, nuclear, power plant and structure engineering fields. Optimal designs of FGM structures have been previously presented in [2, 3, 25].

Cylindrical shells are commonly employed in many engineering and industry applications such as the aerospace, automobile, pressure vessels and ships industries. The free vibration study of these structures is an important aspect of their design procedure. In the past two decades, many researchers studied the free vibration characteristics of FGM cylindrical shells. Some authors used the classical shell theory (CST) to study the free vibration of FGM circular

---

\*Corresponding author. Tel.: +962 772 388 233, e-mail: nabeel963030@yahoo.com.  
<https://doi.org/10.24132/acm.2021.654>

cylindrical shells. For example, Loy et al. [27] were pioneers in the study of the vibration of functionally graded cylindrical shells. They studied FGMs whose constituents have volumetric fraction gradients through the thickness direction based on simple power-law. The governing equations were derived using Love's thin shell theory. The Rayleigh-Ritz method was employed to obtain the eigenvalue equation for simply-supported cylinders. A similar study was conducted by Pradhan et al. [34] for various boundary conditions but with modified expression for a spatial displacement field. A similar approach was adopted by Arshad et al. [4] to investigate the vibration characteristics of FGM cylindrical shells under several types of volumetric fraction laws. Haddadpour et al. [20] researched the free vibration of FGM cylindrical shells through temperature variation. In [20], the material properties were considered to be function of the temperature. The governing equations were obtained on the basis of the Love's shell theory with von Karman-Donnell's nonlinearity type, and the Galerkin method was employed to solve the equations. Using the wave propagation approach, Iqbal et al. [21] investigated the free vibration of FGM cylindrical shells. The first-order shear deformation theory (FSDT) has been adopted by some authors. For example, Tornabene [42] investigated the free vibration of FGM cylindrical shells using the FSDT with the generalized differential quadrature method. The constituents of base materials were considered to vary in the direction of the thickness, in compliance with four-parameter power-law distributions. Su et al. [40] presented a unified solution method for free vibration analysis of functionally graded cylindrical and conical shells and annular plates using FSDT and Rayleigh-Ritz method. A four-parameter power law gradation along the thickness direction for material properties was employed. Kim [24] studied free vibrations of FGM cylindrical shells with material gradient through thickness following the four-parameter power-law. The cylinders were partially resting on an elastic foundation. The motion was represented by having as basis the first-order shear deformation theory. The motion equation for the eigenvalue problem was obtained using Rayleigh-Ritz method as well as the variational approach. Shahbaztabar et al. [38] investigated the free vibrations of FGM cylinders implanted into a Pasternak elastic foundation, based on the first-order shear deformation theory and the Rayleigh-Ritz method. The cylindrical shells were in partial or full contact with a fluid. Recently, Liu et al. [26] investigated the free vibrations characteristics of FGM circular cylinders based on the first-order shear deformation shell theory. The displacements were expressed as wave function expansions. The base materials were considered to vary in the direction of the thickness, in compliance with a four-parameter power-law distribution. Najafizadeh and Isvandzibaei [29] studied the free vibration of FGM thin cylindrical shells with ring supports using third-order shear deformation theory (TSDT), and the governing equations were obtained using an energy functional with the Rayleigh-Ritz method. Matsunaga [28] investigated the vibration and stability of functionally graded cylindrical shells, by means of a two-dimensional higher-order theory. The Hamilton's principle was employed for the derivation of the governing equations, while accounting for the effects of transverse shear, normal deformations, and rotational inertia. By decreasing the number of terms in the power series expansion, several higher-order theories were used to solve the eigenvalue problem. Shen [39] investigated the nonlinear free vibration of FGM cylindrical shells embedded in an outer elastic medium and in thermal environments using Reddy's third order shear deformation theory with von Karman nonlinear kinematics. The equations of motion were solved using perturbation technique. Punera and Kant [35] studied the free vibrations of FGM open cylindrical shells using several higher-order theories. Then, the Navier's method was employed to transform the partial equations into an eigenvalue problem. Elasticity based solutions have been used, as well. Chen et al. [16] investigated the free vibration of simply supported, fluid-filled FGM cylindrical shells. Using the three-dimensional fundamental

equations of anisotropic elasticity, a state equation with variable coefficients was derived in a unified matrix form and a laminate approximate model was employed. Alibeigloo et al. [1] studied the free vibration of piezoelectric layers embedded in a FGM cylindrical shell using the state space method for simply supported boundary conditions and the differential quadrature method for non-simply supported boundary conditions. The constituents of materials were assumed to vary along the thickness according to an exponential law with Poisson's ratio held constant. Jin et al. [22] adopted the first-order shear deformation shell theory model to FGM cylindrical shells. In [22], the Haar-wavelet discretization was employed in the axial direction, and the Fourier series were adopted for the circumferential direction. The partial differential equations were transformed to algebraic equations. Then, the natural frequencies of the FGM cylinders were attained by solving algebraic equations. Ni et al. [31] used the Hamiltonian approach to find the exact solution for the free vibration of FGM circular cylindrical shells embedded in an elastic medium. Based on the Reissner shell theory and symplectic mathematics, solutions were determined analytically. Furthermore, the finite element method was employed by Ram et al. [37] to study the free vibration of a cylindrical shell with a cut out. Golpayegani et al. [19] employed the FEM to determine the natural frequencies of FGM cylinders with a variable thickness.

In the present work, an analysis of a FGM closed circular cylindrical shell is performed using the higher-order shear deformation shell theory and the virtual displacements principle in a strong form based on the collocation of radial basis functions. The eigenvalues governing equation is obtained using the Carrera's unified formulation (CUF) [30]. The CUF was introduced by Carrera [4–15, 30] for multilayered composite structures. Generally, it provides a procedure for implementing many structural theories and finite elements in a unified manner. Another major advantage of the CUF is that the governing equations are expressed in terms of several fundamental nuclei. These nuclei are independent of the order of thickness functions employed in the transverse direction. The CUF was extensively employed in previous studies, more details about it are available, e.g., in [41]. In the present work, the volumetric fractions of the constituents of the base materials follow a conventional power-law distribution through the thickness. The current analysis is examined by comparing the obtained results with those of previous studies. In addition, parametric studies are performed for FGM cylindrical shells considering several boundary conditions in order to show the effect of several design variables on the natural frequencies.

## **2. Functionally graded material**

The FGM circular cylindrical shells employed in this research are made of two materials. The volumetric fractions of the base materials gradually vary in the radial direction of the cylinder in compliance with the simple power-law. The volumetric fraction of the first base material is assumed as

$$V_1(z) = \left( \frac{z}{h} + \frac{1}{2} \right)^P, \quad (1)$$

where  $P \geq 0$  is the power-law exponent,  $h$  is the thickness of the cylinder,  $z$  is the radial coordinate of the cylinder, and  $z \in \left[ -\frac{h}{2}, \frac{h}{2} \right]$ . The volumetric fraction of the second base material is given by  $V_2(z) = 1 - V_1(z)$ . Equivalent material properties are estimated by the Voigt model as

$$E(z) = E_1V_1(z) + E_2V_2(z) = (E_1 - E_2) \left( \frac{z}{h} + \frac{1}{2} \right)^P + E_2, \quad (2)$$

$$\rho(z) = \rho_1V_1(z) + \rho_2V_2(z) = (\rho_1 - \rho_2) \left( \frac{z}{h} + \frac{1}{2} \right)^P + \rho_2, \quad (3)$$

$$\nu(z) = \nu_1V_1(z) + \nu_2V_2(z) = (\nu_1 - \nu_2) \left( \frac{z}{h} + \frac{1}{2} \right)^P + \nu_2, \quad (4)$$

where  $E$  is the modulus of elasticity,  $\rho$  is the mass density,  $\nu$  is the Poisson’s ratio, and the subscripts 1 and 2 refer to materials 1 and 2, respectively. According to (2)–(4), the material properties vary gradually from those of material 1 at the outer surface ( $z = h/2$ ) to those of material 2 at the inner surface ( $z = -h/2$ ). The variations of the volumetric fraction of material 1 through the thickness of the cylinder are shown in Fig. 1.

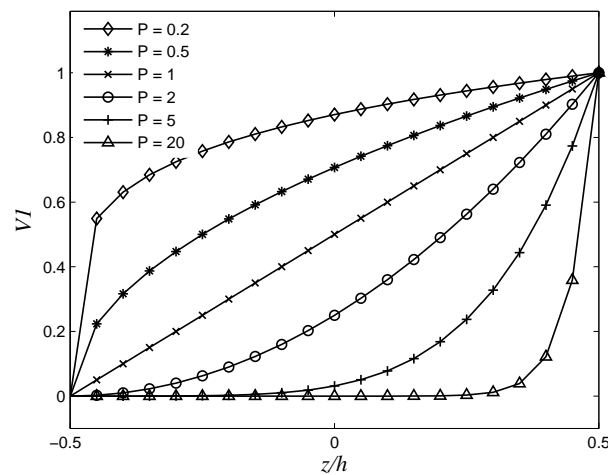


Fig. 1. Variations of the volumetric fraction of the first constituent along the cylinder thickness

### 3. Mathematical formulation

#### 3.1. Governing equations and boundary conditions

Let us consider a circular cylindrical shell shown in Fig. 2, where  $R$  is the radius,  $L$  is the length, and  $h$  is the thickness. In this study, the third-order shear deformation theory was applied while considering transverse shear and rotary inertia. Hence, the displacements can be written in the following polynomial form [36,44]

$$\begin{aligned} u(x, \theta, z, t) &= u_0(x, \theta) + z\psi_\alpha(x, \theta) + z^3\varphi_\alpha(x, \theta), \\ v(x, \theta, z, t) &= v_0(x, \theta) + z\psi_\theta(x, \theta) + z^3\varphi_\theta(x, \theta), \\ w(x, \theta, z, t) &= w_0(x, \theta) + z\psi_z(x, \theta), \end{aligned} \quad (5)$$

where  $u_0$ ,  $v_0$  and  $w_0$  are the middle surface displacements of the shell,  $\psi_\alpha$ ,  $\psi_\theta$ ,  $\psi_z$  are the middle surface rotations, and  $\varphi_\alpha$ ,  $\varphi_\theta$  are three higher-order terms in the Taylor’s series expansion that represents the higher-order transverse deformations field [36,44]. In this section, the fundamental

nuclei, which allow the derivation of the equations of motion and the boundary conditions in compliance with the CUF, are obtained in a strong form [30]. The aim is the collocation of the present radial basis functions, see [23, 30].

The functionally graded shell is divided into a number ( $NL$ ) of uniform-thickness layers. The square of the infinitesimal linear segment in the  $\kappa$ -layer, its associated infinitesimal area and its volume are given by [25]

$$\begin{aligned} df_{\kappa}^2 &= dx^2 + \left(1 + \frac{z}{R}\right) d\theta^2 + dz^2, & d\Omega_{\kappa} &= \left(1 + \frac{z}{R}\right) dx d\theta, \\ dV_{\kappa} &= \left(1 + \frac{z}{R}\right) dx d\theta dz. \end{aligned} \quad (6)$$

Note that the formulation of a shell theory can be followed from [25]. The stresses and strains are split into in-plane and normal components, which are then denoted by the subscripts  $p$  and  $n$ , respectively.

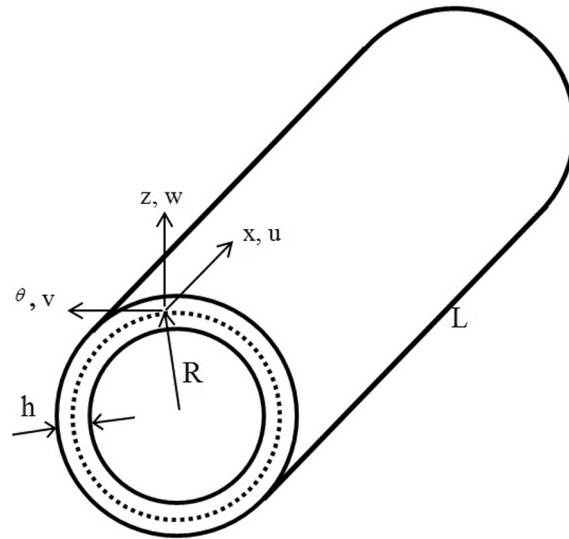


Fig. 2. A circular cylindrical shell

The mechanical strains in the  $\kappa$ -th layer can be related to the displacement field  $u^{(\kappa)} = [u_x^{(\kappa)}, u_{\theta}^{(\kappa)}, u_z^{(\kappa)}]^T$  by the geometrical relations

$$\begin{aligned} \varepsilon_{pG}^{(\kappa)} &= \begin{pmatrix} \varepsilon_{xx}^{(\kappa)} \\ \varepsilon_{\theta\theta}^{(\kappa)} \\ \varepsilon_{x\theta}^{(\kappa)} \end{pmatrix} = (D_p^{(\kappa)} + A_p^{(\kappa)}) u^{(\kappa)}, \\ \varepsilon_{nG}^{(\kappa)} &= \begin{pmatrix} \varepsilon_{xz}^{(\kappa)} \\ \varepsilon_{\theta z}^{(\kappa)} \\ \varepsilon_{zz}^{(\kappa)} \end{pmatrix} = (D_{n\Omega}^{(\kappa)} + D_{nz}^{(\kappa)} - A_n^{(\kappa)}) u^{(\kappa)}, \end{aligned} \quad (7)$$

where  $G$  denotes the geometrical relations. The differential matrix operators  $D_p^{(\kappa)}$ ,  $D_{n\Omega}^{(\kappa)}$ ,  $D_{nz}^{(\kappa)}$ ,  $A_n^{(\kappa)}$  and  $A_p^{(\kappa)}$  are expressed as follows [23]

$$D_{nz}^{(\kappa)} = \begin{bmatrix} \partial z & 0 & 0 \\ 0 & \partial z & 0 \\ 0 & 0 & \partial z \end{bmatrix}, \quad D_p^{(\kappa)} = \begin{bmatrix} \partial x & 0 & 0 \\ 0 & \frac{\partial \theta}{1+z/R} & 0 \\ \frac{\partial \theta}{1+z/R} & \partial x & 0 \end{bmatrix},$$

$$D_{n\Omega}^{(\kappa)} = \begin{bmatrix} 0 & 0 & \frac{\partial x}{1+z/R} \\ 0 & 0 & \frac{\partial \theta}{1+z/R} \\ 0 & 0 & 0 \end{bmatrix}, \quad A_n^{(\kappa)} = \begin{bmatrix} 0 & 0 & 0 \\ 0 & \frac{-1}{R} & 0 \\ 0 & 0 & 0 \end{bmatrix}, \quad A_p^{(\kappa)} \equiv [0].$$

The three-dimensional constitutive equations are given by [36, 44] as

$$\begin{aligned} \sigma_\alpha &= \overline{Q_{11}}\varepsilon_\alpha + \overline{Q_{12}}\varepsilon_\beta + \overline{Q_{13}}\varepsilon_z + \overline{Q_{16}}\gamma_{\alpha\beta}, \\ \sigma_\beta &= \overline{Q_{12}}\varepsilon_\alpha + \overline{Q_{22}}\varepsilon_\beta + \overline{Q_{23}}\varepsilon_z + \overline{Q_{26}}\gamma_{\alpha\beta}, \\ \sigma_\alpha &= \overline{Q_{13}}\varepsilon_\alpha + \overline{Q_{23}}\varepsilon_\beta + \overline{Q_{33}}\varepsilon_z + \overline{Q_{36}}\gamma_{\alpha\beta}, \\ \sigma_{\beta z} &= \overline{Q_{44}}\gamma_{\beta z} + \overline{Q_{45}}\gamma_{\alpha z}, \\ \sigma_{\alpha z} &= \overline{Q_{45}}\gamma_{\beta z} + \overline{Q_{55}}\gamma_{\alpha z}, \\ \sigma_{\alpha\beta} &= \overline{Q_{16}}\varepsilon_\alpha + \overline{Q_{26}}\varepsilon_\beta + \overline{Q_{36}}\varepsilon_z + \overline{Q_{66}}\gamma_{\alpha\beta}. \end{aligned} \tag{8}$$

The case considered in this study is a particular case in which the material has the following properties:  $\overline{Q_{16}} = \overline{Q_{26}} = \overline{Q_{36}} = \overline{Q_{45}} = 0$ . The matrices of the three-dimensional elastic constants  $Q_{pp}^{(\kappa)}$ ,  $Q_{pn}^{(\kappa)}$ ,  $Q_{np}^{(\kappa)}$ , and  $Q_{nn}^{(\kappa)}$  are presented as follows [23, 30, 44]

$$\begin{aligned} Q_{pp}^{(\kappa)} &= \begin{bmatrix} \frac{E^\kappa(1-(\nu^\kappa)^2)}{1-3(\nu^\kappa)^2-2(\nu^\kappa)^3} & \frac{E^\kappa(\nu^\kappa+(\nu^\kappa)^2)}{1-3(\nu^\kappa)^2-2(\nu^\kappa)^3} & 0 \\ \frac{E^\kappa(\nu^\kappa+(\nu^\kappa)^2)}{1-3(\nu^\kappa)^2-2(\nu^\kappa)^3} & \frac{E^\kappa(1-(\nu^\kappa)^2)}{1-3(\nu^\kappa)^2-2(\nu^\kappa)^3} & 0 \\ 0 & 0 & \frac{E^\kappa}{2(1+\nu^\kappa)} \end{bmatrix}, \\ Q_{pp}^{(\kappa)} &= \begin{bmatrix} \frac{E^\kappa}{2(1+\nu^\kappa)} & 0 & 0 \\ 0 & \frac{E^\kappa}{2(1+\nu^\kappa)} & 0 \\ 0 & 0 & \frac{E^\kappa(1-(\nu^\kappa)^2)}{1-3(\nu^\kappa)^2-2(\nu^\kappa)^3} \end{bmatrix}, \\ Q_{pn}^{(\kappa)} &= \begin{bmatrix} 0 & 0 & \frac{E^\kappa(\nu^\kappa+(\nu^\kappa)^2)}{1-3(\nu^\kappa)^2-2(\nu^\kappa)^3} \\ 0 & 0 & \frac{E^\kappa(\nu^\kappa+(\nu^\kappa)^2)}{1-3(\nu^\kappa)^2-2(\nu^\kappa)^3} \\ 0 & 0 & 0 \end{bmatrix}, \\ Q_{np}^{(\kappa)} &= \begin{bmatrix} 0 & 0 & 0 \\ 0 & 0 & 0 \\ \frac{E^\kappa(\nu^\kappa+(\nu^\kappa)^2)}{1-3(\nu^\kappa)^2-2(\nu^\kappa)^3} & \frac{E^\kappa(\nu^\kappa+(\nu^\kappa)^2)}{1-3(\nu^\kappa)^2-2(\nu^\kappa)^3} & 0 \end{bmatrix}. \end{aligned} \tag{9}$$

In this work, the strong form of the governing differential equations and boundary conditions is obtained in terms of displacement components and their derivatives. This is done by means of the principle of virtual displacements (PVD) [17, 30]

$$\delta L_i^{(\kappa)} = \delta L_p^{(\kappa)} + \delta L_\xi^{(\kappa)}. \tag{10}$$

The virtual variation of the strain energy is considered as the sum of two contributes [23, 30, 44]

$$\sum_{k=1}^{N_l} \delta L_i^{(\kappa)} = \sum_{k=1}^{N_l} \int_{A_\kappa} \int_{\Omega_\kappa} \delta \varepsilon_{nG}^{\kappa T} \sigma_{nC}^\kappa \, d\Omega_\kappa \, dz + \sum_{k=1}^{N_l} \int_{A_\kappa} \int_{\Omega_\kappa} \delta \varepsilon_{pG}^{\kappa T} \sigma_{pC}^\kappa \, d\Omega_\kappa \, dz, \tag{11}$$

where  $\Omega_\kappa$  and  $A_\kappa$  are the integration domains in the  $(x, \theta)$  plane and the  $z$ -direction, respectively. Here  $T$  denotes the transposition of the relevant vector,  $\delta L_i^{(\kappa)}$  is the external work for the  $\kappa$ -th layer, and  $C$  denotes the constitutive equations.

The three displacement components  $u_x$ ,  $u_\theta$ , and  $u_z$  and their relative variations can be modelled as [30]

$$\begin{aligned} (u_x, u_\theta, u_z) &= F_\tau(u_{x\tau}, u_{\theta\tau}, u_{z\tau}), \\ (\delta u_x, \delta u_\theta, \delta u_z) &= F_\tau(\delta u_{x\tau}, \delta u_{\theta\tau}, \delta u_{z\tau}), \end{aligned} \tag{12}$$

where  $F_\tau$  are the functions of the thickness coordinate  $z$ , and  $\tau$  is the sum index. By resorting to the displacement field in (8), the vectors  $F_\tau = [1 \ z \ z^3]$  are selected for the displacements  $u$ ,  $v$ ,  $w$ . Then, all the terms of the motion equations are obtained by integrating through the thickness direction.

By replacing the geometrical relations (7), the material constitutive equations (8), and the approximation of the displacement components (5), and after integrating by parts (11), the governing equations for the  $\kappa$ -th layer shell subjected to mechanical loadings are given as

$$K_{uu}^\kappa u_\tau^\kappa - M^\kappa \ddot{u}_\tau^\kappa = 0, \tag{13}$$

where the double dots denote the accelerations, and the fundamental nucleus  $K_{uu}^{(\kappa\tau s)}$  is obtained in the form [23, 30]

$$K_{uu}^{(\kappa\tau s)} = \int_{A_\kappa} \begin{bmatrix} (A_p - D_p)^T Q_{pp}^{(\kappa)} (A_p + D_p) + \\ (A_p - D_p)^T Q_{pn}^{(\kappa)} (D_{n\Omega} + D_{nz} - A_n) + \\ (-D_{n\Omega} + D_{nz} - A_n)^T Q_{np}^{(\kappa)} (A_p + D_p) + \\ (-D_{n\Omega} + D_{nz} - A_n)^T Q_{nn}^{(\kappa)} (D_{n\Omega} + D_{nz} - A_n) \end{bmatrix} F_\tau F_s \left(1 + \frac{z}{R}\right) dz, \tag{14}$$

where  $\int_{A_\kappa} \dots dz = \int_{-h_\kappa/2}^{h_\kappa/2} \dots dz$ ,

$$\begin{aligned} (K_{uu}^{\kappa\tau s})_{11} &= -\frac{E^\kappa(1 - (\nu^\kappa)^2)}{1 - 3(\nu^\kappa)^2 - 2(\nu^\kappa)^3} J_{\beta/\alpha}^{\kappa\tau s} \partial_\alpha^s \partial_\alpha^\tau - \frac{E^\kappa}{2(1 + \nu^\kappa)} J_{\alpha/\beta}^{\kappa\tau s} \partial_\beta^s \partial_\beta^\tau + \\ &\quad \frac{E^\kappa}{2(1 + \nu^\kappa)} (J_{\alpha\beta}^{\kappa\tau s z} - J_\beta^{\kappa\tau s} - J_\beta^{\kappa\tau s z} + J_{\beta/\alpha}^{\kappa\tau s}), \\ (K_{uu}^{\kappa\tau s})_{12} &= -\frac{E^\kappa(\nu^\kappa + (\nu^\kappa)^2)}{1 - 3(\nu^\kappa)^2 - 2(\nu^\kappa)^3} J^{\kappa\tau s} \partial_\alpha^\tau \partial_\beta^s - \frac{E^\kappa}{2(1 + \nu^\kappa)} J^{\kappa\tau s} \partial_\alpha^s \partial_\beta^\tau, \\ (K_{uu}^{\kappa\tau s})_{13} &= -\frac{E^\kappa(1 - (\nu^\kappa)^2)}{1 - 3(\nu^\kappa)^2 - 2(\nu^\kappa)^3} J_{\beta/\alpha}^{\kappa\tau s} \partial_\alpha^\tau - \frac{E^\kappa(\nu^\kappa + (\nu^\kappa)^2)}{1 - 3(\nu^\kappa)^2 - 2(\nu^\kappa)^3} \frac{1}{R} J_{\alpha\alpha}^{\kappa\tau s} \partial_\alpha^\tau - \\ &\quad \frac{E^\kappa(\nu^\kappa + (\nu^\kappa)^2)}{1 - 3(\nu^\kappa)^2 - 2(\nu^\kappa)^3} J_\beta^{\kappa\tau s} \partial_\alpha^\tau + \frac{E^\kappa}{2(1 + \nu^\kappa)} (J_\beta^{\kappa\tau s} \partial_\alpha^s - J_{\beta/\alpha}^{\kappa\tau s} \partial_\alpha^s), \\ (K_{uu}^{\kappa\tau s})_{21} &= -\frac{E^\kappa(\nu^\kappa + (\nu^\kappa)^2)}{1 - 3(\nu^\kappa)^2 - 2(\nu^\kappa)^3} J^{\kappa\tau s} \partial_\alpha^s \partial_\beta^\tau - \frac{E^\kappa}{2(1 + \nu^\kappa)} J^{\kappa\tau s} \partial_\alpha^\tau \partial_\beta^s, \\ (K_{uu}^{\kappa\tau s})_{22} &= -\frac{E^\kappa}{2(1 + \nu^\kappa)} J_{\beta/\alpha}^{\kappa\tau s} \partial_\alpha^s \partial_\alpha^\tau + \frac{E^\kappa}{2(1 + \nu^\kappa)} \left( J_{\alpha\beta}^{\kappa\tau s z} - \frac{1}{R} J_\alpha^{\kappa\tau s} - \frac{1}{R} J_\alpha^{\kappa\tau s z} + \frac{1}{R^2} J_{\alpha/\beta}^{\kappa\tau s} \right), \\ (K_{uu}^{\kappa\tau s})_{23} &= -\frac{E^\kappa(\nu^\kappa + (\nu^\kappa)^2)}{1 - 3(\nu^\kappa)^2 - 2(\nu^\kappa)^3} J_{\beta\beta}^{\kappa\tau s} \partial_\beta^\tau - \frac{E^\kappa(\nu^\kappa + (\nu^\kappa)^2)}{1 - 3(\nu^\kappa)^2 - 2(\nu^\kappa)^3} J_\alpha^{\kappa\tau s} \partial_\beta^\tau + \\ &\quad \frac{E^\kappa}{2(1 + \nu^\kappa)} \left( J_\alpha^{\kappa\tau s} \partial_\beta^s - \frac{1}{R} J_{\alpha/\beta}^{\kappa\tau s} \partial_\beta^s \right), \end{aligned}$$

$$\begin{aligned}
 (K_{uu}^{\kappa\tau s})_{31} &= \frac{E^\kappa(1 - (\nu^\kappa)^2)}{1 - 3(\nu^\kappa)^2 - 2(\nu^\kappa)^3} J_{\beta/\alpha}^{\kappa\tau} \partial_\alpha^s + \frac{E^\kappa(\nu^\kappa + (\nu^\kappa)^2)}{1 - 3(\nu^\kappa)^2 - 2(\nu^\kappa)^3} \left( \frac{1}{R} J_\alpha^{\kappa\tau} \partial_\alpha^s + J_\beta^{\kappa\tau z s} \partial_\alpha^s \right) - \\
 &\quad \frac{E^\kappa}{2(1 + \nu^\kappa)} (J_\beta^{\kappa\tau s z} \partial_\alpha^\tau - J_{\beta/\alpha}^{\kappa\tau s} \partial_\alpha^\tau), \\
 (K_{uu}^{\kappa\tau s})_{32} &= \frac{E^\kappa(\nu^\kappa + (\nu^\kappa)^2)}{1 - 3(\nu^\kappa)^2 - 2(\nu^\kappa)^3} J_{\beta k}^{\kappa\tau s} \partial_\beta^s + \frac{E^\kappa(\nu^\kappa + (\nu^\kappa)^2)}{1 - 3(\nu^\kappa)^2 - 2(\nu^\kappa)^3} J_\alpha^{\kappa\tau z s} \partial_\beta^s - \\
 &\quad \frac{E^\kappa}{2(1 + \nu^\kappa)} \left( J_\alpha^{\kappa\tau s z} \partial_\beta^\tau - \frac{1}{R} J_{\alpha/\beta}^{\kappa\tau s} \partial_\beta^\tau \right), \\
 (K_{ul}^{\kappa\tau s})_{33} &= \frac{E^\kappa(1 - (\nu^\kappa)^2)}{1 - 3(\nu^\kappa)^2 - 2(\nu^\kappa)^3} + \frac{E^\kappa(1 - (\nu^\kappa)^2)}{1 - 3(\nu^\kappa)^2 - 2(\nu^\kappa)^3} J_{\alpha\beta}^{\kappa\tau z s} + \\
 &\quad 2 \frac{E^\kappa(\nu^\kappa + (\nu^\kappa)^2)}{1 - 3(\nu^\kappa)^2 - 2(\nu^\kappa)^3} \frac{1}{R} J_1^{\kappa\tau s} + \frac{E^\kappa(\nu^\kappa + (\nu^\kappa)^2)}{1 - 3(\nu^\kappa)^2 - 2(\nu^\kappa)^3} (J_\beta^{\kappa\tau z s} + J_\beta^{\kappa\tau s z}) + \\
 &\quad \frac{E^\kappa(\nu^\kappa + (\nu^\kappa)^2)}{1 - 3(\nu^\kappa)^2 - 2(\nu^\kappa)^3} \frac{1}{R} (J_\alpha^{\kappa\tau z s} + J_\alpha^{\kappa\tau z}) - C_{44}^\kappa J_{\alpha/\beta}^{\kappa\tau s} \partial_\beta^s \partial_\beta^\tau - \frac{E^\kappa}{2(1 + \nu^\kappa)} J_{\beta/\alpha}^{\kappa\tau s} \partial_\alpha^s \alpha_\alpha^\tau,
 \end{aligned}$$

where

$$\begin{aligned}
 (J^{\kappa\tau s}, J_\alpha^{\kappa\tau s}, J_\beta^{\kappa\tau s}, J_{\alpha/\beta}^{\kappa\tau s}, J_{\beta/\alpha}^{\kappa\tau s}, J_{\alpha\beta}^{\kappa\tau s}) &= \int_{A_\kappa} F_\tau F_s \cdot \\
 &\quad \left( 1, 1, 1 + \frac{z}{R}, \frac{1}{1 + \frac{z}{R}}, 1 + \frac{z}{R}, 1 + \frac{z}{R} \right) dz, \\
 (J^{\kappa\tau z s}, J_\alpha^{\kappa\tau z s}, J_\beta^{\kappa\tau z s}, J_{\alpha/\beta}^{\kappa\tau z s}, J_{\beta/\alpha}^{\kappa\tau z s}, J_{\alpha\beta}^{\kappa\tau z s}) &= \int_{A_\kappa} \frac{\partial F_\tau}{\partial z} F_s \cdot \\
 &\quad \left( 1, 1, 1 + \frac{z}{R}, \frac{1}{1 + \frac{z}{R}}, 1 + \frac{z}{R}, 1 + \frac{z}{R} \right) dz, \\
 (J^{\kappa\tau s z}, J_\alpha^{\kappa\tau s z}, J_\beta^{\kappa\tau s z}, J_{\alpha/\beta}^{\kappa\tau s z}, J_{\beta/\alpha}^{\kappa\tau s z}, J_{\alpha\beta}^{\kappa\tau s z}) &= \int_{A_\kappa} F_\tau \frac{\partial F_s}{\partial z} \cdot \\
 &\quad \left( 1, 1, 1 + \frac{z}{R}, \frac{1}{1 + \frac{z}{R}}, 1 + \frac{z}{R}, 1 + \frac{z}{R} \right) dz, \\
 (J^{\kappa\tau z s z}, J_\alpha^{\kappa\tau z s z}, J_\beta^{\kappa\tau z s z}, J_{\alpha/\beta}^{\kappa\tau z s z}, J_{\beta/\alpha}^{\kappa\tau z s z}, J_{\alpha\beta}^{\kappa\tau z s z}) &= \int_{A_\kappa} \frac{\partial F_\tau}{\partial z} \frac{\partial F_s}{\partial z} \cdot \\
 &\quad \left( 1, 1, 1 + \frac{z}{R}, \frac{1}{1 + \frac{z}{R}}, 1 + \frac{z}{R}, 1 + \frac{z}{R} \right) dz,
 \end{aligned}$$

and  $M^\kappa$  is the fundamental nucleus for the inertial term given by

$$\begin{aligned}
 M_{11}^{(\kappa\tau s)} &= M_{22}^{(\kappa\tau s)} = M_{33}^{(\kappa\tau s)} = \rho^\kappa J_{x\theta}^{(\kappa\tau s)}, \\
 M_{12}^{(\kappa\tau s)} &= M_{13}^{(\kappa\tau s)} = M_{22}^{(\kappa\tau s)} = M_{23}^{(\kappa\tau s)} = M_{31}^{(\kappa\tau s)} = M_{32}^{(\kappa\tau s)} = 0,
 \end{aligned} \tag{15}$$

where  $\rho^\kappa$  is the mass density of the  $\kappa$ -th layer, and  $J_{x\theta}^{(\kappa\tau s)} = \int_{A_\kappa} F_\tau F_s \left( 1 + \frac{z}{R} \right) dz_\kappa$ .

The Navier-type closed form solution [23, 30, 41] is applied to obtain the natural frequencies of the FGM circular cylinder shell. Placement of the Navier-type closed form solution into the governing equation (13) results in an algebraic system of ordinary differential equations in the time domain, which can be written as an eigenvalue problem. The resulting equations can be

written in the following matrix form

$$\left| \overline{K_{uu}^{(\kappa Ts)}} - \left( \overline{K_{u\sigma}^{(\kappa Ts)}} \left( \overline{K_{u\sigma}^{(\kappa Ts)}} \right)^{-1} \overline{K_{\sigma u}^{(\kappa Ts)}} \right) - \lambda \overline{M_{ij}^{(\kappa Ts)}} \right| = 0, \text{ where } \lambda = \omega_{mn}^2.$$

The above eigenvalue equation can be solved for the various eigenvalues and associated eigenvectors, and the lowest eigenvalue gives the square of the fundamental frequency of vibration.

### 3.2. Collocation with radial basis functions

We apply collocation with radial basis functions to interpolate the algebraic form of the motion equations. Unless otherwise stated, a Chebyshev grid is employed [13, 18, 23, 30]. For all the examples presented in this paper, the following Wendland function is considered

$$\phi(x) = (1 - cr)^8 + (32(cr)^3 + 25(cr)^2 + 8cr + 1),$$

where the shape parameter is obtained by an optimization procedure, as detailed in the study by Ferreira and Fasshauer [18].

## 4. Results and discussion

The method discussed in Section 3 is herein employed to study the free vibration of a circular cylindrical shell composed by FGMs, whose material properties vary through the thickness in compliance with the simple power-law. In this section, a validation study is conducted. Then, a parametric study is performed to investigate the influence of different parameters on the natural frequencies of FGM cylindrical shells.

### 4.1. Validation studies

The accuracy and efficacy of the proposed approach are examined by comparing the present results of the free vibration of FGM cylindrical shells with other results published in previous studies. The FGM considered here is composed of stainless steel and nickel. The material constituents vary through the thickness of the cylinders according to a simple power-law (1). The material properties of the stainless steel are  $E_{st} = 207.788$  GPa,  $\nu_{st} = 0.317756$ , and  $\rho_{st} = 8166$  kg/m<sup>3</sup>. The material properties of the nickel are  $E_{ni} = 205.098$  GPa,  $\nu_{ni} = 0.31$ , and  $\rho_{ni} = 8900$  kg/m<sup>3</sup>. Tables 1 and 2 show comparisons of the natural frequencies of simply-supported FGM cylindrical shells with those of Loy et al. [27], Jin et al. [22], and Xiang et al. [43]. The dimensions of the cylindrical shells are: radius ( $R$ ) = 1 m, length to radius ratio ( $L/R$ ) = 20, thickness to radius ratio ( $h/R$ ) = 0.05 (results in Table 1), and  $h/R = 0.002$  (results in Table 2). The circular cylinders have stainless steel on their inner surface and nickel on their outer surface. Table 3 shows comparisons of the natural frequencies of clamped-clamped FGM cylindrical shells made with those of Iqbal et al. [21] and Ni et al. [31]. The circular cylinders have stainless steel on their outer surface and nickel on their inner surface. The results of [21, 27, 43] are based on the classical shell theory, while the results of [22, 31] are based on the elasticity approach. As can be seen from Tables 1–3, the current results are in good agreement with the existing results of [22, 27, 31, 43].

Table 1. Natural frequencies [Hz] of a circular cylindrical shell with circumferential wave number  $n$  for SS–SS end conditions with  $h/R = 0.05$ ,  $L/R = 20$ , and  $R = 1$  m

$P$		$n$									
		1	2	3	4	5	6	7	8	9	10
0.5	Present	13.123	32.142	89.712	171.791	277.58	407.47	560.71	737.44	937.94	1162.09
	Ref. [27]	13.126	32.151	89.818	171.970	277.95	407.62	560.94	737.87	938.42	1162.60
	Ref. [43]	13.114	32.038	89.716	171.870	277.85	407.53	560.85	737.78	938.33	1162.50
2	Present	13.342	32.678	91.201	174.639	282.46	414.24	570.09	749.87	953.57	1181.27
	Ref. [27]	13.344	32.683	91.309	174.830	282.57	414.39	570.25	750.13	954.00	1181.90
	Ref. [43]	13.337	32.579	91.211	174.740	282.47	414.30	570.16	750.03	953.90	1181.80
15	Present	13.525	33.148	92.545	177.201	286.46	420.16	578.17	760.41	967.06	1198.18
	Ref. [27]	13.528	33.157	92.617	177.330	286.61	420.31	578.40	760.84	967.63	1198.80
	Ref. [43]	13.512	33.041	92.517	177.230	286.51	420.22	578.31	760.74	967.53	1198.70
30	Present	13.547	33.214	92.727	177.481	287.00	420.97	579.14	761.77	968.84	1200.19
	Ref. [27]	13.549	33.221	92.795	177.660	287.15	421.12	579.50	762.30	969.48	1201.00
	Ref. [43]	13.528	33.120	92.692	177.570	287.05	421.03	579.40	762.19	969.38	1201.00

Table 2. Natural frequencies [Hz] of a circular cylindrical shell with circumferential wave number  $n$  for SS–SS end conditions with  $h/R = 0.002$ ,  $L/R = 20$ , and  $R = 1$  m

$P$		$n$									
		1	2	3	4	5	6	7	8	9	10
0.5	Present	13.103 3	4.441 6	4.119 8	6.979 4	11.152 0	16.334 0	22.488 5	29.616 2	37.732 4	46.858 9
	Ref. [27]	13.103 0	4.438 2	4.115 2	6.975 4	11.145 0	16.317 0	22.447 0	29.524 0	37.548 0	46.517 0
	Ref. [22]	13.104 0	4.440 8	4.118 0	6.977 0	11.146 0	16.317 0	22.447 0	29.524 0	37.547 0	46.514 0
2	Present	13.321 2	4.515 5	4.188 2	7.095 2	11.336 8	16.604 8	22.861 1	30.107 4	38.358 6	47.351 5
	Ref. [27]	13.321 0	4.511 4	4.182 7	7.090 5	11.329 0	16.587 0	22.454 0	30.014 0	38.171 0	47.288 0
	Ref. [22]	13.322 0	4.514 1	4.185 5	7.092 2	11.330 0	16.587 0	22.818 0	30.013 0	38.170 0	47.285 0
15	Present	13.505 5	4.578 1	4.247 9	7.197 3	11.499 9	16.844 2	23.190 4	30.535 9	38.910 4	48.322 4
	Ref. [27]	13.505 0	4.575 9	4.245 1	7.194 3	11.494 0	16.827 0	23.147 0	30.446 0	38.720 0	47.968 0
	Ref. [22]	13.506 0	4.578 6	4.247 9	7.195 9	11.494 0	16.827 0	23.147 0	30.445 0	38.718 0	47.965 0
30	Present	13.526 3	4.585 4	4.255 8	7.211 2	11.522 6	16.876 7	23.235 6	30.600 4	38.986 2	48.416 6
	Ref. [27]	13.526 0	4.583 6	4.253 6	7.208 5	11.516 0	16.859 0	23.192 0	30.505 0	38.795 0	48.061 0
	Ref. [22]	13.527 0	4.586 3	4.256 4	7.210 1	11.517 0	16.859 0	23.192 0	30.504 0	38.793 0	48.058 0

#### 4.2. Parametric studies

To acquire some knowledge regarding the natural frequencies of FGM cylindrical shells, it is important to study the effect of selected design parameters, such as the power-law exponent ( $P$ ), the circumferential wave number ( $n$ ), the length to radius ratio ( $L/R$ ), and the thickness to radius ratio ( $h/R$ ), on these natural frequencies. The radius of the cylinder is assumed constant and equal to 1 m. In the subsequent examples, the FGM circular cylindrical shells are composed of a metal as a first base material and of a ceramic as a second base material. The material properties of the constituents are summarized in Table 4, where the material properties vary through the cylinder thickness in accordance with (2)–(4). The considered boundary conditions are SS–SS, C–C, and C–F.

Table 3. Natural frequencies [Hz] of a circular cylindrical shell with circumferential wave number  $n$  for C–C end conditions with  $h/R = 0.002$ ,  $L/R = 20$ , and  $R = 1$  m

$P$		$n$				
		1	2	3	4	5
0.3	Present	27.221 30	9.647 00	5.888 20	7.526 30	11.513 30
	Ref. [31]	27.210 68	9.644 38	5.893 39	7.530 45	11.509 20
	Ref. [21]	28.999 60	9.784 30	5.907 20	7.536 10	11.515 20
1	Present	26.860 90	9.517 50	5.807 20	7.422 00	11.354 00
	Ref. [31]	26.847 68	9.516 27	5.815 10	7.430 80	11.352 61
	Ref. [21]	28.613 20	9.654 74	5.830 10	7.435 40	11.358 90
10	Present	26.336 40	9.330 60	5.694 00	7.276 00	11.129 40
	Ref. [31]	26.328 10	9.331 21	5.701 22	7.281 33	11.124 85
	Ref. [21]	28.049 60	9.462 32	5.711 01	7.284 56	11.131 00
15	Present	26.300 80	9.318 00	5.686 10	7.264 80	11.112 00
	Ref. [31]	26.299 63	9.316 97	5.694 10	7.267 10	11.103 50
	Ref. [21]	28.011 40	9.449 00	5.701 80	7.272 31	11.112 60

Table 4. Material properties of FGM constituents

Property	Metal (Aluminum)	Ceramic (Alumina)
$E$ [GPa]	70	350
$\rho$ [kg/m <sup>3</sup> ]	2 700	3 900
$\nu$	0.3	0.24

Figs. 3–5 show the variations of the natural frequencies with the changes of the circumferential wave number  $n$  and the power-law exponent  $P$ , assuming that  $L/R = 20$  and  $h/R = 0.05$ . It can be noted that the natural frequencies of the FGM cylinders increase with increasing power-law exponent in all considered boundary conditions. This was expected because increasing the power-law exponent decreases the amount of aluminum and increases the amount of alumina, which has a greater modulus of elasticity. Moreover, it can be noted that at a high wave number, the natural frequencies for all the considered boundary conditions, are close to each other. However, at low wave numbers, the natural frequencies of the C–C boundary conditions are the greatest, followed by those of the SS–SS boundary conditions and then by those of the C–F boundary conditions.

The variations of the fundamental frequency [Hz] with the length to radius ( $L/R$ ) ratio and the power-law exponent are shown in Figs. 6–8 (the thickness to radius ratio is constant and equals to 0.05). As shown for  $L/R \leq 5$ , increasing the length or decreasing the radius of the FGM cylinders significantly decreases the fundamental frequency. Also for the low values of the  $L/R$  ratio, the power-law exponent effect was great, but this effect decreases with increasing  $L/R$  ratio. Moreover, it is obvious that by increasing the  $L/R$  ratio, the influence of the boundary conditions decreases, and the fundamental frequencies become close to each other when  $L/R \geq 20$ .

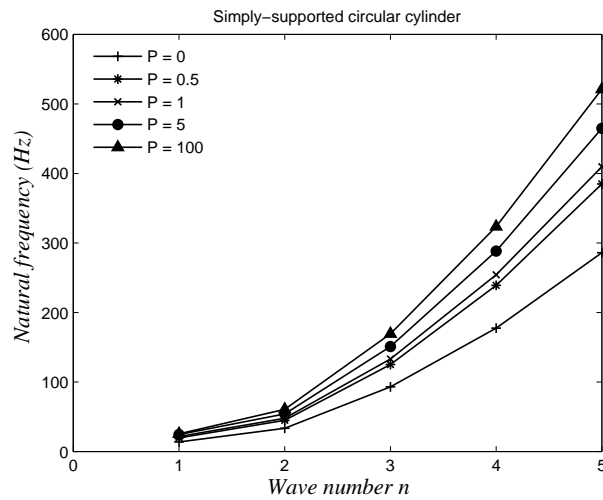


Fig. 3. Variations of the natural frequencies [Hz] with circumferential wave number  $n$  for SS–SS FGM cylindrical shell ( $L/R = 20$ , and  $h/R = 0.05$ )

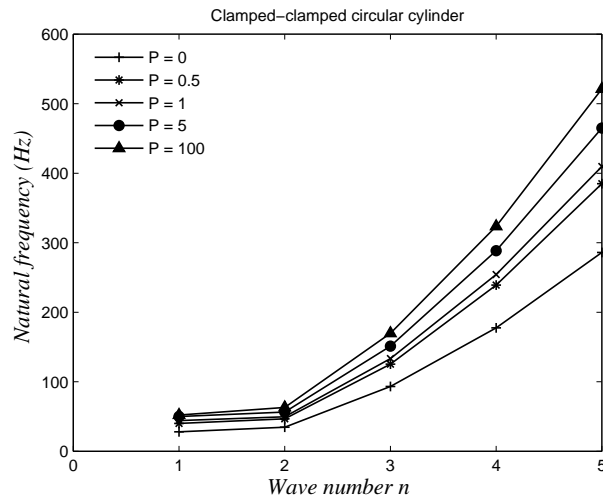


Fig. 4. Variations of the natural frequencies [Hz] with circumferential wave number  $n$  for C–C FGM cylindrical shell ( $L/R = 20$ , and  $h/R = 0.05$ )

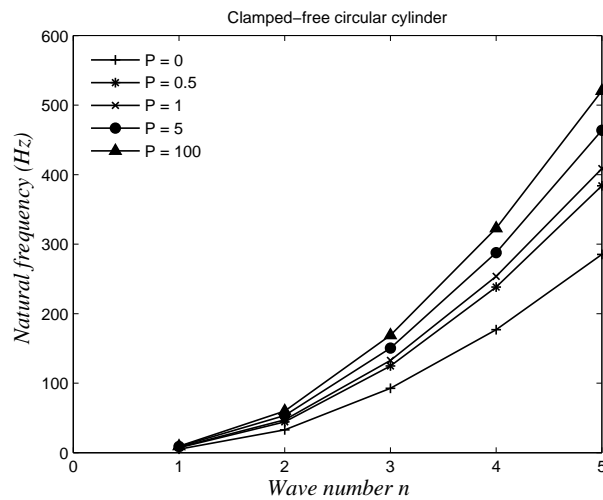


Fig. 5. Variations of the natural frequencies [Hz] with circumferential wave number  $n$  for C–F FGM cylindrical shell ( $L/R = 20$ , and  $h/R = 0.05$ )

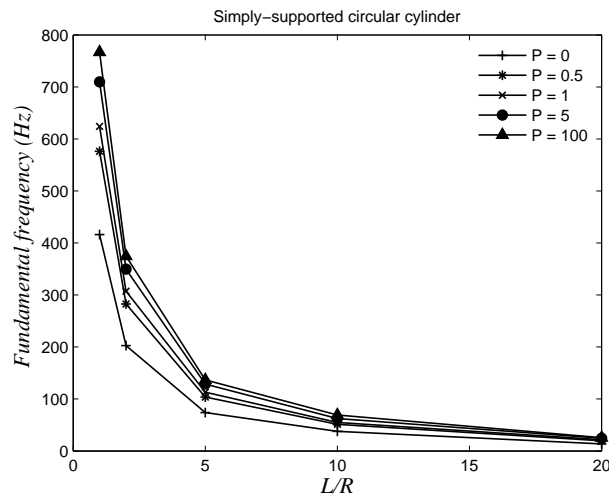


Fig. 6. Variations of the fundamental frequencies [Hz] with  $L/R$  ratio for SS–SS FGM cylindrical shell ( $h/R = 0.05$ )

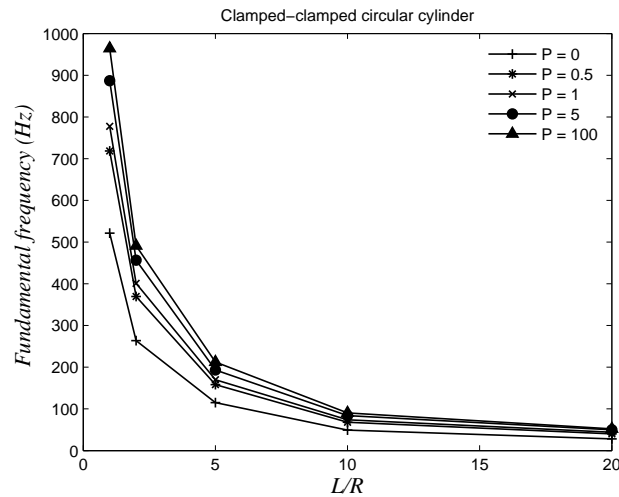


Fig. 7. Variations of the fundamental frequencies [Hz] with  $L/R$  ratio for C–C FGM cylindrical shell ( $h/R = 0.05$ )

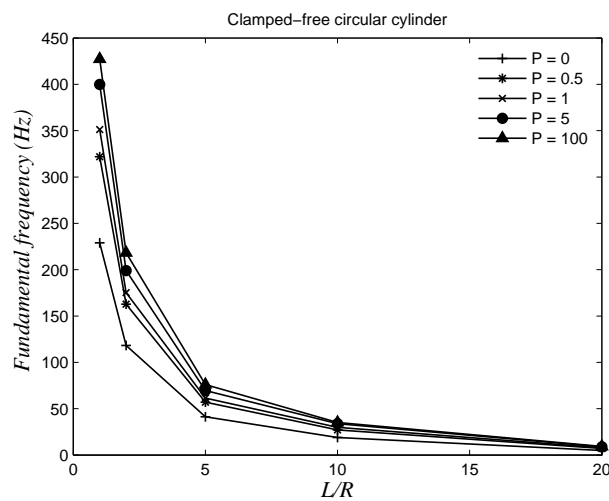


Fig. 8. Variations of the fundamental frequencies [Hz] with  $L/R$  ratio for C–F FGM cylindrical shell ( $h/R = 0.05$ )

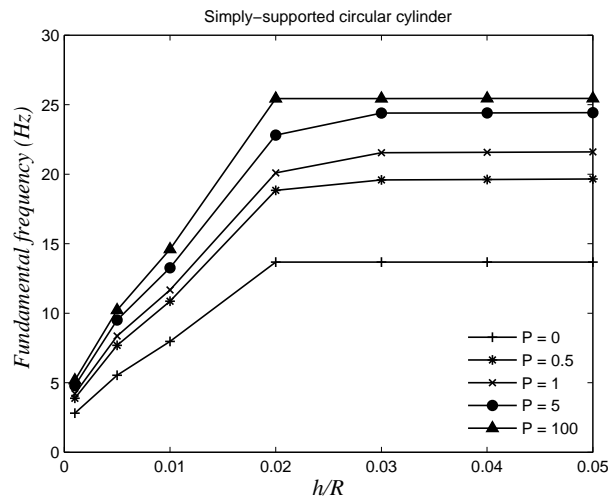


Fig. 9. Variations of the fundamental frequencies [Hz] against  $h/R$  ratio for SS–SS FGM cylindrical shell ( $L/R = 20$ )

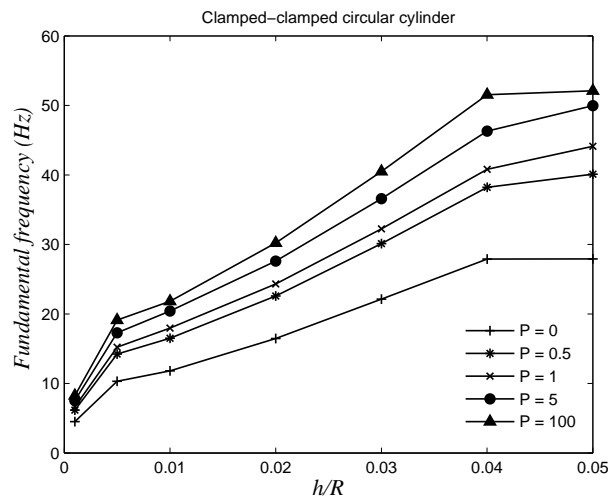


Fig. 10. Variations of the fundamental frequencies [Hz] with  $h/R$  ratio for C–C FGM cylindrical shell ( $L/R = 20$ )

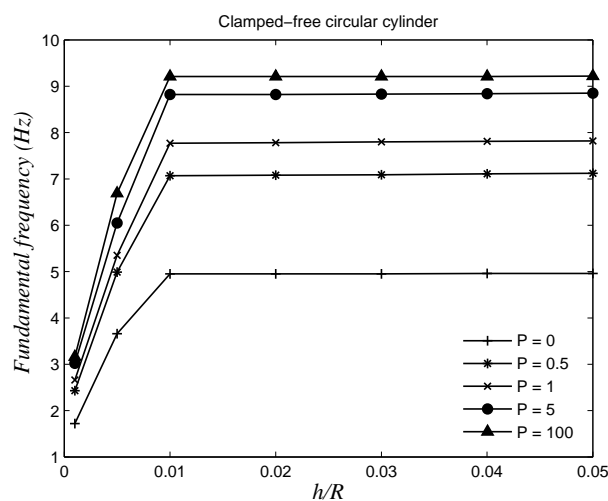


Fig. 11. Variations of the fundamental frequencies [Hz] against  $h/R$  ratio for C–F FGM cylindrical shell ( $L/R = 20$ )

Figs. 9–11 show the variations of the fundamental frequencies [Hz] with the thickness to radius ( $h/R$ ) ratio and the power-law exponent. The length to radius ratio was considered to be constant (i.e.,  $L/R = 20$ ). As shown in the figures, all the cylinders with the different boundary conditions show similar trends. By increasing the  $h/R$  ratio, the fundamental frequency increases to a certain limit. Then, any additional increase in the  $h/R$  ratio would not result in any noticeable increase in the frequencies. In all cases of different geometries and boundary conditions of the FGM cylindrical shells, the natural frequencies have intermediate values between those of the cylindrical shells composed by aluminum and alumina.

## 5. Conclusion

In this work, the free vibration of FGM circular cylindrical shells was investigated for different boundary conditions such as SS–SS, C–C, and C–F. The material volumetric fractions were varied through the thickness, in compliance with the simple power-law and the Voigt model was adopted to evaluate the equivalent material properties. Moreover, the third-order shear deformation shell theory was employed with the Carrera's unified formulation to derive the equations governing the free vibrations of circular cylindrical shells. The presented numerical results were validated by comparing them with results published in previous studies. In addition, the effects of the power-law exponent, the circumferential wave number, the length to radius ratio as well as the thickness to radius ratio on the natural frequencies of the FGM circular cylindrical shells were studied. Overall, the conducted parametric study should provide a guide for design engineers.

The future extension of this work will investigate the natural frequencies of FGM cylindrical shells considering other volumetric fraction laws as well as the design of FGM cylindrical shells with optimal natural frequencies.

## References

- [1] Alibeigloo, A., Kani, A., Pashaei, M., Elasticity solution for the free vibration analysis of functionally graded cylindrical shell bonded to thin piezoelectric layers, *International Journal of Pressure Vessels and Piping* 89 (2012) 98–111. <https://doi.org/10.1016/j.ijpvp.2011.10.020>
- [2] Alshabatat, N., Myers, K., Naghshineh, K., Design of in-plane functionally graded material plates for optimal vibration performance, *Noise Control Engineering Journal* 64 (2) (2016) 268–278. <https://doi.org/10.3397/1/376377>
- [3] Alshabatat, N., Naghshineh, K., Optimization of natural frequencies and sound power of beams using functionally graded material, *Advances in Acoustics and Vibration* (2014) Article ID 752361. <https://doi.org/10.1155/2014/752361>
- [4] Arshad, S., Naeem, M., Sultana, N., Frequency analysis of functionally graded material cylindrical shells with various volume fraction laws, *Proceedings of the Institution of Mechanical Engineers, Part C: Journal of Mechanical Engineering Science* 221 (2007) 1483–1495. <https://doi.org/10.1243/09544062JMES738>
- [5] Carrera, E., A Reissner's mixed variational theorem applied to vibration analysis of multilayered shells, *Journal of Applied Mechanics* 66 (1) (1999) 69–78. <https://doi.org/10.1115/1.2789171>
- [6] Carrera, E., A Study of transverse normal stress effects on vibration of multilayered plates and shells, *Journal of Sound and Vibration* 225 (1) (1999) 803–829. <https://doi.org/10.1006/jsvi.1999.2271>

- [7] Carrera, E.,  $C_z^0$  requirements-models for the two dimensional analysis of multilayered structures, *Composite Structures* 37 (3) (1997) 373–383. [https://doi.org/10.1016/S0263-8223\(98\)80005-6](https://doi.org/10.1016/S0263-8223(98)80005-6)
- [8] Carrera, E., Evaluation of layerwise mixed theories for laminated plates analysis, *AIAA Journal* 36 (5) (1998) 830–839. <https://doi.org/10.2514/2.444>
- [9] Carrera, E., Layer-wise mixed models for accurate vibrations analysis of multilayered plates, *Journal of Applied Mechanics* 65 (4) (1998) 820–828. <https://doi.org/10.1115/1.2791917>
- [10] Carrera, E., Mixed layer-wise models for multilayered plates analysis, *Composite Structures* 43 (1) (1998) 57–70. [https://doi.org/10.1016/S0263-8223\(98\)00097-X](https://doi.org/10.1016/S0263-8223(98)00097-X)
- [11] Carrera, E., Multilayered shell theories accounting for layerwise mixed description, Part 1: Governing equations, *AIAA Journal* 37 (9) (1999) 1107–1116. <https://doi.org/10.2514/2.821>
- [12] Carrera, E., Multilayered shell theories accounting for layerwise mixed description, Part 2: Numerical evaluations, *AIAA Journal* 37 (9) (1999) 1117–1124. <https://doi.org/10.2514/2.822>
- [13] Carrera, E., Brischetto, S., Nali, P., *Plates and shells for smart structures: Classical and advanced theories for modeling and analysis*, John Wiley & Sons, 2011. <https://doi.org/10.1002/9781119950004>
- [14] Carrera, E., Cinefra, M., Petrolo, M., Zappino, E., *Finite element analysis of structures through unified formulation*, John Wiley & Sons, 2014. <https://doi.org/10.1002/9781118536643>
- [15] Carrera, E., Giunta, G., Petrolo, M., *Beam structures: Classical and advanced theories*, John Wiley & Sons, 2011. <https://doi.org/10.1002/9781119978565>
- [16] Chen, W. Q., Bian, Z. G., Ding, J., Three-dimensional vibration analysis of fluid-filled orthotropic FGM cylindrical shells, *International Journal of Mechanical Sciences* 46 (1) (2004) 159–171. <https://doi.org/10.1016/j.ijmecsci.2003.12.005>
- [17] Ferreira, A., Carrera, E., Cinefra, M., Roque, C., Polit, O., Analysis of laminated shells by a sinusoidal shear deformation theory and radial basis functions collocation, accounting for through-the-thickness deformations, *Composites Part B: Engineering* 42 (5) (2011) 1276–1284. <https://doi.org/10.1016/j.compositesb.2011.01.031>
- [18] Ferreira, A., Fasshauer, G., Computation of natural frequencies of shear deformable beams and plates by a RBF pseudo spectral method, *Computer Methods in Applied Mechanics and Engineering* 196 (1–3) (2006) 134–146. <https://doi.org/10.1016/j.cma.2006.02.009>
- [19] Golpayegani, I., Arani, E., Foroughifar, A., Finite element vibration analysis of variable thickness thin cylindrical FGM shells under various boundary conditions, *Materials Performance and Characterization* 8 (1) (2019) 491–502. <https://doi.org/10.1520/MPC20180148>
- [20] Haddadpour, H., Mahmoudkhani, S., Navazi, H. M., Free vibration analysis of functionally graded cylindrical shells including thermal effects, *Thin-Walled Structures* 45 (6) (2007) 591–599. <https://doi.org/10.1016/j.tws.2007.04.007>
- [21] Iqbal, Z., Naeem, M. N., Sultana, N., Vibration characteristics of FGM circular cylindrical shells using wave propagation approach, *Acta Mechanica* (208) (2009) 237–248. <https://doi.org/10.1007/s00707-009-0141-z>
- [22] Jin, G., Xie, X., Liu, Z., The Haar wavelet method for free vibration analysis of functionally graded cylindrical shells based on the shear deformation theory, *Composite Structures* 108 (1) (2014) 435–448. <https://doi.org/10.1016/j.compstruct.2013.09.044>
- [23] Jing, H., Tzeng, K. G., Refined shear deformation theory of laminated shells, *AIAA Journal* (31) (4) (1993) 765–773. <https://doi.org/10.2514/3.11615>
- [24] Kim, Y. W., Free vibration analysis of FGM cylindrical shell partially resting on Pasternak elastic foundation with an oblique edge, *Composites: Part B* 70 (1) (2015) 263–276. <https://doi.org/10.1016/j.compositesb.2014.11.024>
- [25] Kraus, H., *Thin elastic shells: An introduction to the theoretical foundations and the analysis of their static and dynamic behavior*, John Wiley & Sons, New York, 1967.

- [26] Liu, T., Wang, A., Wang, Q., Qin, B., Wave based method for free vibration characteristics of functionally graded cylindrical shells with arbitrary boundary conditions, *Thin-Walled Structures* 148 (1) (2020). <https://doi.org/10.1016/j.tws.2019.106580>
- [27] Loy, C., Lam, K., Reddy, J., Vibration of functionally graded cylindrical shells, *International Journal of Mechanical Sciences* 41 (1) (1999) 309–324. [https://doi.org/10.1016/S0020-7403\(98\)00054-X](https://doi.org/10.1016/S0020-7403(98)00054-X)
- [28] Matsunaga, H., Free vibration and stability of functionally graded circular cylindrical shells according to a 2D higher-order deformation theory, *Composite Structures* 88 (1) (2009) 519–531. <https://doi.org/10.1016/j.compstruct.2008.05.019>
- [29] Najafizadeh, M. M., Isvandzibaei, M. R., Vibration of functionally graded cylindrical shells based on higher order shear deformation plate theory with ring support, *Acta Mechanica* (191) (2007) 75–91. <https://doi.org/10.1007/s00707-006-0438-0>
- [30] Neves, A. M., Ferreira, A. J. M., Carrera, E., Cinefra, M., Roque, C. M. C., Jorge, R. M. N., Soares, C. M. M., Free vibration analysis of functionally graded shells by a higher-order shear deformation theory and radial basis functions collocation, accounting for through-the-thickness deformations, *European Journal of Mechanics-A/Solids* (37) (2013) 24–34. <https://doi.org/10.1016/j.euromechsol.2012.05.005>
- [31] Ni, Y., Tong, Z., Rong, D., Zhou, Z., Xu, X., A new Hamiltonian-based approach for free vibration of a functionally graded orthotropic circular cylindrical shell embedded in an elastic medium, *Thin-Walled Structures* (120) (2017) 236–248. <https://doi.org/10.1016/j.tws.2017.09.003>
- [32] Niino, M., Hirai, T., Watanabe, R., The functionally gradient materials, *Journal of the Japan Society for Composite Materials* 13 (1) (1987) 257–264. <https://doi.org/10.6089/jscm.13.257>
- [33] Nikbakht, S., Kamarian, S., Shakeri, M., A review on optimization of composite structures, Part II: Functionally graded materials, *Composite Structures* 214 (1) (2019) 83–102. <https://doi.org/10.1016/j.compstruct.2019.01.105>
- [34] Pradhan, S. C., Loy, C. T., Lam, K. Y., Reddy, J. N., Vibration characteristics of functionally graded cylindrical shells under various boundary conditions, *Applied Acoustics* 61 (1) (2000) 111–129. [https://doi.org/10.1016/S0003-682X\(99\)00063-8](https://doi.org/10.1016/S0003-682X(99)00063-8)
- [35] Punera, D., Kant, T., Free vibration of functionally graded open cylindrical shells based on several refined higher order displacement models, *Thin-Walled Structures* 119 (1) (2017) 707–726. <https://doi.org/10.1016/j.tws.2017.07.016>
- [36] Qatu, M., Zannon, M., Mainuddin, G., Application of laminated composite materials in vehicle design: Theories and analyses of composite shells, *SAE International Journal of Passenger Cars-Mechanical Systems* 6 (2) (2013) 1347–1353. <https://doi.org/10.4271/2013-01-1989>
- [37] Ram, K., Pratyusha, K., Kiranmayi, P., Free vibration of functionally graded cylindrical shell panel with and without a cutout, *Journal of Solid Mechanics* 10 (3) (2018) 672–687.
- [38] Shahbatabar, A., Izadi, A., Sadeghian, M., Kazemi, M., Free vibration analysis of FGM circular cylindrical shells resting on the Pasternak foundation and partially in contact with stationary fluid, *Applied Acoustics* 153 (1) (2019) 87–101. <https://doi.org/10.1016/j.apacoust.2019.04.012>
- [39] Shen, H. S., Nonlinear vibration of shear deformable FGM cylindrical shells surrounded by an elastic medium, *Composite Structures* (94) (3) (2012) 1144–1154. <https://doi.org/10.1016/j.compstruct.2011.11.012>
- [40] Su, Z., Jin, G., Shi, S., Ye, T., Jia, X., A unified solution for vibration analysis of functionally graded cylindrical, conical shells and annular plates with general boundary conditions, *International Journal of Mechanical Sciences* (80) (2014) 62–80. <https://doi.org/10.1016/j.ijmecsci.2014.01.002>
- [41] Thai, H. T., Kim, S. E., A review of theories for the modeling and analysis of functionally graded plates and shells, *Composite Structures* 128 (1) (2015) 70–86. <https://doi.org/10.1016/j.compstruct.2015.03.010>

- [42] Tornabene, F., Free vibration analysis of functionally graded conical, cylindrical shell and annular plate structures with a four-parameter power-law distribution, *Computer Methods in Applied Mechanics and Engineering* 198 (37–40) (2009) 11–35. <https://doi.org/10.1016/j.cma.2009.04.011>
- [43] Xiang, S., Li, G.C., Zhang, W., Yang, M.S., Natural frequencies of rotating functionally graded cylindrical shells, *Applied Mathematics and Mechanics* (33) (2012) 345–56. <https://doi.org/10.1007/s10483-012-1554-6>
- [44] Zannon, M., Fundamental frequency of laminated composite thick spherical shells, *Journal of Mathematics Research* 11 (1) (2019) 57–63. <https://doi.org/10.5539/jmr.v11n1p57>